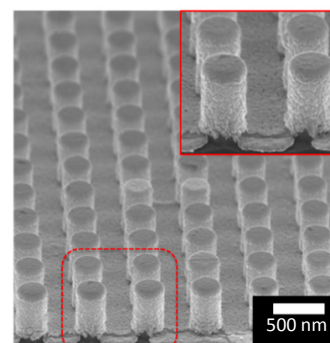




# Hybrid metal-insulator-metal structures on Si nanowires array for surface enhanced Raman scattering

Kaichen Xu<sup>1,2†</sup>, Chentao Zhang<sup>3†</sup>, Tzu Hsiao Lu<sup>2</sup>,  
Puqun Wang<sup>1</sup>, Rui Zhou<sup>3</sup>, Rong Ji<sup>2\*</sup> and Minghui Hong<sup>1\*</sup>

<sup>1</sup>Department of Electrical and Computer Engineering, National University of Singapore, 4 Engineering Drive 3, 117576, Singapore; <sup>2</sup>Data Storage Institute, (A\*STAR) Agency for Science Technology and Research, 2 Fusionopolis Way, 138634, Singapore; <sup>3</sup>Department of Mechanical and Electrical Engineering, Xiamen University, Xiamen 361005, China



**Abstract:** Surface enhanced Raman scattering (SERS) is an efficient technique to detect low concentration molecules. In this work, periodical silicon nanowires (SiNWs) integrated with metal-insulator-metal (MIM) layers are employed as SERS substrates. Laser interference lithography (LIL) combined with reactive ion etching (RIE) is used to fabricate large-area periodic nanostructures, followed by decorating the MIM layers. Compared to MIM disks array on Si surface, the SERS enhancement factor (EF) of the MIM structures on the SiNWs array can be increased up to 5 times, which is attributed to the enhanced electric field at the boundary of the MIM disks. Furthermore, high density of nanoparticles and nanogaps serving as hot spots on sidewall surfaces also contribute to the enhanced SERS signals. Via changing the thickness of the insulator layer, the plasmonic resonance can be tuned, which provides a new localized surface plasmon resonance (LSPR) characteristic for SERS applications.

**Keywords:** surface-enhanced Raman scattering; nanostructure fabrication; plasmonics; metal-insulator-metal  
**DOI:** 10.3969/j.issn.1003-501X.2017.02.006

**Citation:** *Opto-Elec Eng*, 2017, **44**(2): 185–191

## 1 Introduction

Surface enhanced Raman spectroscopy (SERS) has attracted a great amount of research interests in the past decades due to its fascinating use for detecting single molecules<sup>[1]</sup>. Two main mechanisms, chemical and electromagnetic enhancement, are used to explain the SERS phenomenon<sup>[2]</sup>. In particular, the latter mechanism is widely accepted as the dominated effect. Owing to the electromagnetic field enhancement from localized surface plasmons (LSPs), various SERS-active substrates with strong and robust SERS enhancement have been reported<sup>[3-6]</sup>. In recent years, a new kind of intriguing platforms built from “elevated” cavity or bowtie arrays has been developed for reliable SERS detections<sup>[7-8]</sup>. Known as the lightning-rod effect, bowtie nanoantenna arrays are able to confine the optical radiation into

nanoscale volumes, performing excellent field concentration, which can exhibit distinct SERS effect due to strong LSP resonance in the vicinity of sharp nanotips of nanoparticles and small gaps among neighboring nanoparticles<sup>[9]</sup>. The “elevated” properties make the cavity or bowtie decouple from the substrate, which is expected to enhance near-field intensity<sup>[8]</sup>. However, such “elevated” nanocavity array is limited to the weak tunability of plasmonic resonance and complicated fabrication processes, such as electron-beam lithography (EBL) and focused ion beam (FIB) milling<sup>[8-10]</sup>. Their main disadvantages of high cost and slow throughput are not practical for SERS applications.

To resolve these issues, metal-insulator-metal (MIM) system is one of good candidates. Featuring as its ability to confine excited surface plasmons and coupled photons in the dielectric layer sandwiched by two metal disks, the MIM configuration provides a tunable characteristic of LSP resonance to enhance Raman signals<sup>[11-12]</sup>. Most of MIM platforms are developed on glass substrates, in which substrate effect is not taken into consideration<sup>[11-13]</sup>. Recently, several semiconductor materials, in

Received 12 November 2016; accepted 10 December 2016

† These authors contributed equally to this work

\* E-mail: Ji\_Rong@dsi.-a-star.edu.sg, elehmh@nus.edu.sg

particular, silicon with high refractive index ( $>3.5$ ) combined with low extinction coefficient in a portion of the visible spectrum and in the near-infrared region have been employed as building blocks for SERS applications [14]. Li et al proposed a 3-D resonant cavity antenna based on Si nanopillar arrays, where the disk backplane is for vertical plasmonic cavity [15]. Polemi et al investigated the optical properties of Si pillars that support plasmonic nanoparticles [16]. Furthermore, the SERS performances of silver decorated SiNWs array by LIL at different aspect ratios are discussed to optimize the Raman signals by balancing the large detection area and light trapping effect [17-18]. However, to the best of our knowledge, the SERS performance based on the system of the MIM layers integrated on SiNWs array has not been investigated.

In this paper, the hybrid MIM disks on Si nanowires array are studied. The nanostructures are fabricated by LIL and RIE. The SERS performance of the MIM disks on SiNWs at different thicknesses of  $\text{SiO}_2$  layer is demonstrated in comparison with those of MIM disks array and the single Au disks array on Si surfaces. The advantages of integrating MIM layers on the SiNWs are the enhancement of electric field at the edge of MIM disks and plenty of nanoparticles serving as hot spots on the sidewall surface of SiNWs, which increase the intensity of Raman signals. Furthermore, the existing SiNWs create larger surface areas, which improve the adsorption of probing molecules within the detection volume.

## 2 Design and fabrication

As shown in Fig. 1, to fabricate the hybrid MIM disks on the SiNWs array, a positive photoresist S1805 is spin-coated at 5000 r/m for 30 s on the p-type Si (100) substrate, followed by a prebake at 95 °C for 1 min. Then the substrate is exposed twice by LIL with a 90° rotation of the sample between the two exposures. After the photoresist develops, a post-bake at 110 °C for 15 min is done

to strengthen the photoresist. RIE is then utilized to transfer the photoresist patterns onto the Si substrate to obtain SiNWs array with 100 sccm  $\text{CHF}_3$  and 15 sccm  $\text{SF}_6$  as working gas for 90 s. Finally, residual photoresist on the top of SiNWs is washed away by immersing it in acetone solution. A 25 nm thick gold layer is deposited on the Si substrate by sputtering, then a layer of  $\text{SiO}_2$  is evaporated by chemical vapor deposition (CVD) over the gold layer at the thickness of 0, 10, 20 and 30 nm, followed by the deposition of another 15 nm thick gold layer. On the bottom of the layer is 2 nm Cr to increase the adhesion between MIM disks and Si substrate. For comparison of the MIM disks on SiNWs array to MIM disks on Si surface and Au disks on Si surface in terms of SERS performance, other two nanostructures are also prepared, following by the same LIL with negative photoresist, MIM deposition and lift-off processes.

To characterize the fabricated nanostructures, a field emission scanning electron microscope (FESEM) is used to observe the morphology of the samples. Hybrid SERS substrates are functionalized with a self-assembled monolayer of 4-methylbenzenethiol (4-MBT) [19]. The substrates are submerged inside a 10 mM 4-MBT solution made with ethanol for 8 hours to allow the formation of self-assembled monolayer and then rinsed in an ethanol solution for 30 s, followed by nitrogen drying. To evaluate the SERS properties of the substrates, a Renishaw 2000 Raman Imaging Microscope is applied with laser excitation wavelength at 532 nm. Raman signals are obtained through a  $50\times$  ( $NA=0.8$ ) microscope lens and detected by a thermoelectrical CCD array.

The simulation is carried out by using the finite-difference-time-domain (FDTD) method (FDTD Solutions 7.5, Lumerical Inc.). A broadband plane wave ranging from 400 nm to 1000 nm is used to excite the structure in  $z$  direction with perfectly matched layers conditions. Periodic boundary conditions are applied to a unit cell in  $x$  and  $y$  directions.

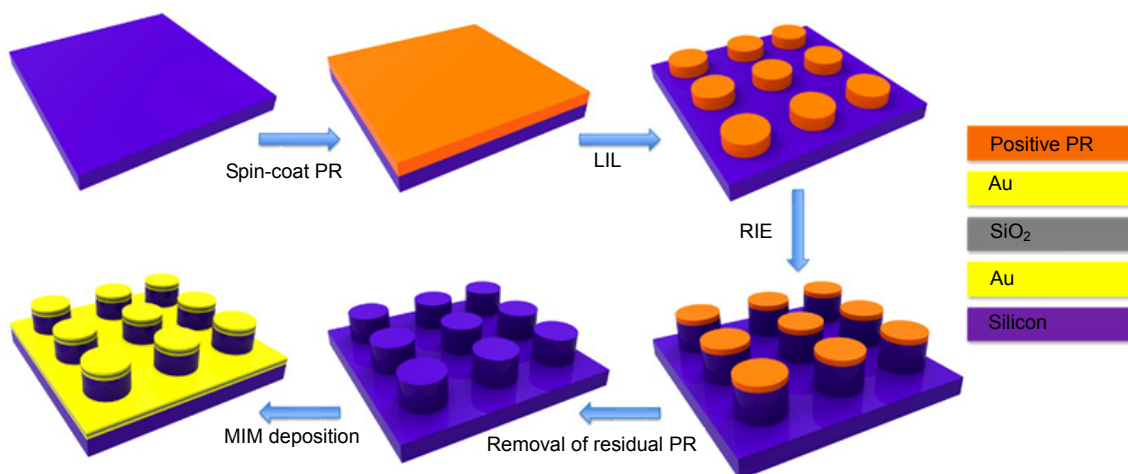


Fig. 1 Schematic of the fabrication procedures of MIM disks on SiNWs array by laser interference lithography and reactive ion etching.

### 3 Results and discussion

#### 3.1 Nanostructures fabrication

Fig. 2(a) shows the SEM images of well-ordered SiNWs array fabricated by LIL. The height and period of cylindrical shapes of the structures can be well controlled by etching time and exposure dose. Fig. 2(b) illustrates the SEM images of the MIM disks on SiNWs array. It can be seen that uniform and continuous films can be observed on the top of SiNWs. On the sidewall surface of SiNWs, discontinuous metal films are formed, which create a high density of nanoparticles serving as hot spots. Meanwhile, a SiO<sub>2</sub> layer sandwiched between two Au layers on the bottom of SiNWs array can be clearly observed because of the contrast difference.

To demonstrate the unique properties of the hybrid MIM disks on the SiNWs array for enhancing Raman signals, Fig. 3(a) shows the SERS spectra of monolayer 4-MBT molecules adsorbed on nanostructures of Au disks array on Si surface, MIM disks array on Si surface and hybrid MIM disks on SiNWs array. 4-MBT molecules have two characteristic Raman bands at 1083 cm<sup>-1</sup> and 1575 cm<sup>-1</sup>, corresponding to the in-plane ring-breathing mode coupled with the C-S mode and the C-C stretching mode [12]. The broad band at 900~1000 cm<sup>-1</sup> comes from the silicon substrate [20]. To compare the surface Raman enhancement on these platforms, the enhancement factor (EF) is estimated by the intensity of the SERS signals normalized with respect to that of the non-SERS signals using the equation (1):

$$EF = \frac{I_{\text{SERS}}}{N_{\text{SERS}}} \times \frac{I_0}{N_0}, \quad (1)$$

where  $N_{\text{SERS}}$  and  $N_0$  are the numbers of molecules contributing to the SERS and non-SERS signals,  $I_{\text{SERS}}$  and  $I_0$  the intensities of the specified Raman band (1083 cm<sup>-1</sup> and 1575 cm<sup>-1</sup>) from 4-MBT molecules adsorbed on the SERS substrates. To determine  $N_0$ , following the approach

of Cai et al [21], the number of probed molecules is obtained by using a thin sample cell containing solution of 4-MBT. Therefore,  $N_0$  can be calculated as:

$$N_0 = NA \cdot \frac{\rho h A}{M}, \quad (2)$$

where  $NA$  is Avogadro's number,  $\rho$  volume density and  $M$  molar mass of 4-MBT,  $h$  the thickness of the SERS sample and  $A$  the spot area. For  $N_{\text{SERS}}$ , the 4-MBT surface density is assumed as  $4.5 \times 10^{14}$  molecules/cm<sup>2</sup>. The calculation can be summarized as equation (3):

$$N_{\text{SERS}} = \rho_s \cdot \frac{S_{\text{gold}} A}{P^2}, \quad (3)$$

where  $\rho_s$  is the surface packing density,  $S_{\text{gold}}$  the surface area accounting for the top surface as well as the side walls for each nanopillar or nanodisk,  $A$  the spot area and  $P$  the period of the nanostructures array. It should be noted that due to the same objective lens used in both Raman and SERS experiment, the spot area can be cancelled out in the EF calculation [12].

#### 3.2 SERS spectra of MIM disks on SiNWs array & Si surface and Au disks array on Si surfaces

From Fig. 3 and Table 1, the calculated SERS EF of the hybrid MIM disks on the SiNWs array can provide roughly 5 times larger than those of the MIM disks and Au disks array on Si surface. For the platform of Au disks array on Si surface, the weak intensity of Raman signals is due to the limited electric hot spots, which are mainly located at the edge of Au disks [22]. However, the edges are not sharp, resulting in the weak enhancement of incident light. Meanwhile, for the MIM disks array on Si surface, the SERS EF is slightly larger than that of the Au disks array on Si surface, which is attributed to the LSPRs at the top edge of Au disks as well as the local electric field around the insulator layers coupled by two metal disks. However, the efficient surface area of the MIM disks array on Si surface limits the light-matter interaction among incident light, molecules and metal particles. For

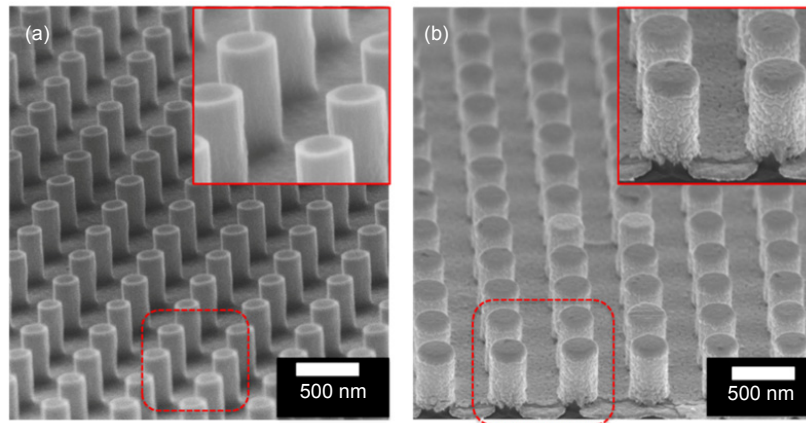


Fig. 2 SEM images (tilt-view 70°) of the fabricated (a) SiNWs array and (b) MIM disks on SiNWs array. The figures in the top right corner of Figs. 2(a) and (b) show the corresponding selected areas.

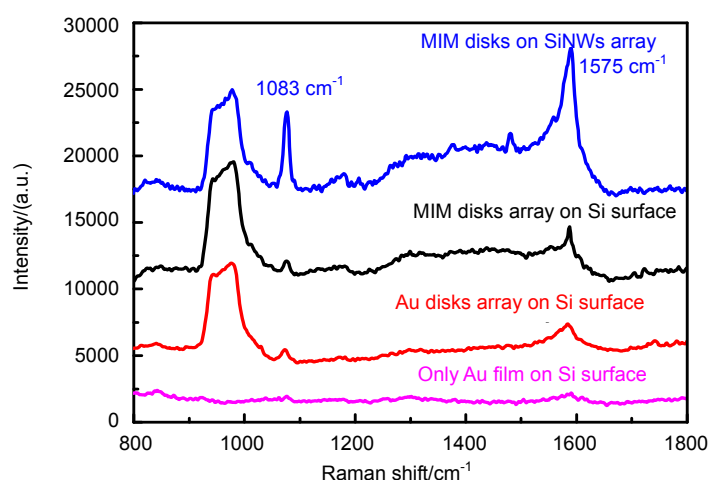


Fig. 3 SERS spectra of 4-MBT molecules adsorbed on 50 nm thick Au film on Si surface, Au disks array on Si surface, MIM disks array on Si surface and MIM disks on SiNWs array. Thickness of Au disks is 50 nm and Au-SiO<sub>2</sub>-Au layers 25-20-25 nm. All the period is 500 nm and height of SiNWs is ~400 nm.

Table 1 Calculated SERS enhancement factors. Thickness of Au disks is 50 nm and Au-SiO<sub>2</sub>-Au layers 25-20-25 nm. All the period is 500 nm and height of SiNWs is ~400 nm.

Raman bands	Au disks array on Si surface	MIM disks array on Si surface	MIM disks on SiNWs array
1083 cm <sup>-1</sup>	$5.37 \times 10^5$	$7.96 \times 10^5$	$2.79 \times 10^6$
1575 cm <sup>-1</sup>	$1.44 \times 10^6$	$1.70 \times 10^6$	$3.64 \times 10^6$

the hybrid MIM disks on SiNWs array, it has more efficient surface areas available for the formation of high density hot spots generated at the nanoparticles on the sidewalls of SiNWs. Furthermore, the existing SiNWs array improves the adsorption of probing molecules within the detection volume and light scattering within the SiNWs. Therefore, the SERS performance for other two nanostructures is poorer than that of MIM disks on SiNWs array.

### 3.3 Numerical simulation

In this work, FDTD numerical simulation is performed to investigate the optical properties of the hybrid nanostructures. Fig. 4 illustrates the schematic models of four different designs and the corresponding calculated electric field distribution (Log scale) at the excitation wavelength of 532 nm. The thickness of the bottom and top Au layers is 25 nm, while the SiO<sub>2</sub> layer is 20 nm and the diameter for the SiNWs is 200 nm with period 500 nm and height 400 nm.

For the MIM disks array on Si surface, the intensity of the maximum localized field is weaker than that of MIM disks on the SiNWs array in Figs. 4(b) and 4(d). This phenomenon is because the existing SiNWs introduce constructive interference among the incident and reflective light and the bottom metallic film boosts the light scattering intensity, both of which lead to the enhanced electric field intensity. In addition, the metallic nanoparticles serving as the hot spots on sidewall surface may

also contribute to SERS signals. Although the maximum localized field of only Au disks on the SiNWs array is similar to that of MIM disks on the SiNWs array, the enhanced electric field can be excited on both Au disks for the MIM disks on the SiNWs array. Therefore, the hybrid MIM disks on the SiNWs array with bottom metallic layers are the optimal design among the four models for the SERS applications. The simulation shows that electric field enhancement is dependent on the height of SiNWs, which demonstrates a periodic variation of around 250 nm pillar height (see the appendix). These results guide us to precisely engineer pillars supported plasmonic nanostructures by both considering electric field enhancement and high aspect ratio of SiNWs with large areas for the SERS applications.

### 3.4 Influence of SiO<sub>2</sub> thickness

Fig. 5 and Table 2 show the SERS spectra of monolayer 4-MBT adsorbed on the MIM disks on the SiNWs array with variable thickness of SiO<sub>2</sub> layer. It can be seen that the MIM disks on the SiNWs array with 30 nm thick SiO<sub>2</sub> layer exhibit the strongest SERS *EF*, which is ~ 2 times larger than those with 0, 10 and 20 nm thick SiO<sub>2</sub> layers in terms of Raman bands at 1083 cm<sup>-1</sup> and 1575 cm<sup>-1</sup>. For the MIM disks array on the SiNWs array with a fixed disk diameter, plasmonic resonance can be controlled by changing the thickness of the SiO<sub>2</sub> layer, which leads to a blueshift of LSP resonance when the thickness of the SiO<sub>2</sub> layer is increased<sup>[23]</sup>. Such phenomenon can be explained

by a dipole-dipole interaction spring model<sup>[24]</sup>. The frequency of each spring can be considered as the resonance frequency of each gold disk. When two gold disks are placed layer by layer and separated by a SiO<sub>2</sub> film serving as the gap, the MIM disks with the larger gap weaken the

attractive forces between the two isolated nanodisks, leading to a higher resonance frequency than that with the smaller gap. Therefore, for the MIM disks on the SiNWs array with the thicker SiO<sub>2</sub>, the intensity of excited photons is enhanced as well as the Raman signals.

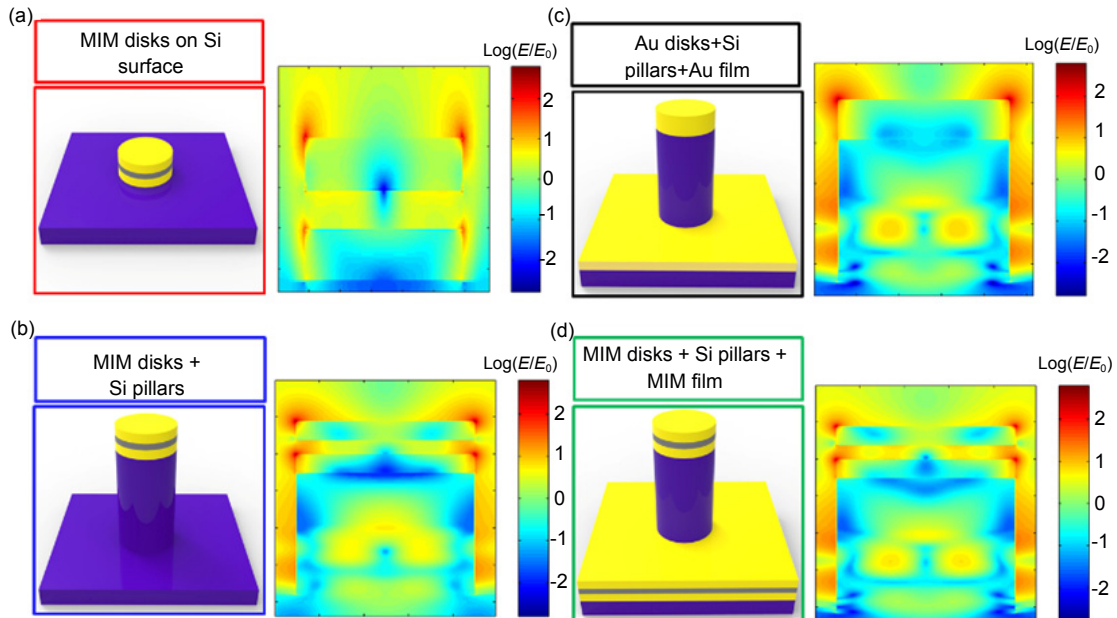


Fig. 4 Calculated electric field distribution (Log scale) at the excitation wavelength of 532 nm. (a) MIM disks array on Si surface. (b) MIM disks on SiNWs array without bottom metallic layers. (c) Only Au disks on SiNWs array with bottom metallic layers and (d) MIM disks on the SiNWs array with bottom MIM layers.

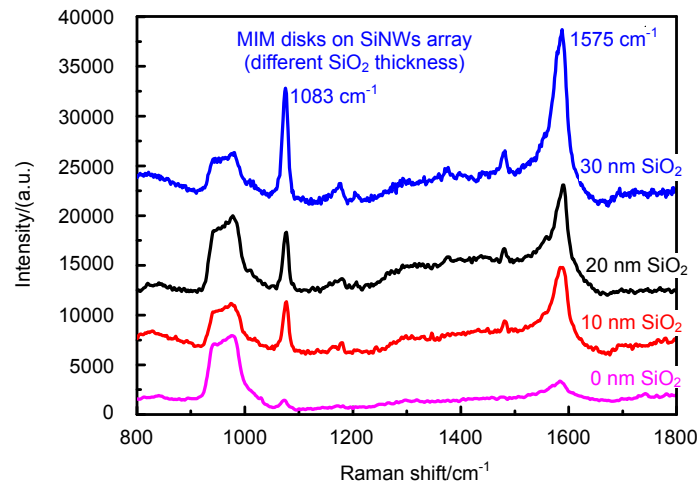


Fig. 5 SERS spectra of 4-MBT adsorbed on the MIM disks on SiNWs array at different thickness of SiO<sub>2</sub> layer.

Table 2 Calculated SERS enhancement factors for MIM disks on SiNWs array. The height of SiNWs is around 400 nm. Thickness of both Au layers is 25 nm.

Raman bands	MIM disks on SiNWs array			
	0 nm SiO <sub>2</sub>	10 nm SiO <sub>2</sub>	20 nm SiO <sub>2</sub>	30 nm SiO <sub>2</sub>
1083 cm <sup>-1</sup>	3.29×10 <sup>5</sup>	2.42×10 <sup>6</sup>	2.79×10 <sup>6</sup>	5.20×10 <sup>6</sup>
1575 cm <sup>-1</sup>	5.61×10 <sup>5</sup>	3.02×10 <sup>6</sup>	3.64×10 <sup>6</sup>	7.08×10 <sup>6</sup>

Particularly, when the thickness of SiO<sub>2</sub> layer is 0 nm, which can be seen as only 50 nm thick Au films deposited on SiNWs array, the intensities of Raman shifts at 1083 cm<sup>-1</sup> and 1575 cm<sup>-1</sup> both decrease sharply by around 15 times, indicating that SiNWs array integrated with MIM layers plays a more significant role than that integrated with only Au layers in SERS detection. Although the EF of Au disks array on Si surface is nearly three times larger than that of Au disks on SiNWs array, the efficient surface area is different for these two structures.

In this work, nanoparticles are introduced on sidewall surface of the SiNWs. In order to clearly explain the effect of thickness of the SiO<sub>2</sub> layer on the performance of SERS, MIM layers can be firstly deposited on the Si surface, followed by surface patterning by LIL and then RIE. During this procedure, only MIM layers are formed on the top of the SiNWs with clean sidewall and bottom surface.

## 4 Conclusions

In summary, hybrid SERS substrates based on highly ordered SiNWs array as building blocks integrated with MIM configuration are designed and fabricated. By combining LIL and RIE, well-ordered and cylindrical shapes of SiNWs array are fabricated over a large area (cm<sup>2</sup>). After MIM layers deposition by the sputtering process, the SERS performance of MIM disks on SiNWs array exhibits around 5 times enhancement in comparison with those of MIM disks and Au disks array on Si surface. This phenomenon is attributed to the enhancement of electric field at the edge of MIM disks and plenty of nanoparticles serving as hot spots on the sidewall surfaces of SiNWs. Meanwhile, SiNWs array boosts the adsorption of probing molecules within the detection volume and light scattering within the SiNWs. Plasmon resonant wavelength can be possibly matched to excita-

tion wavelength by changing the thickness of the dielectric layer. These factors contribute to the enhanced SERS signals. This 3D platform with large area, good periodicity and pillar height dependent electric field enhancement can provide guidance for further optimizing and engineering such “elevated” plasmonic nanostructures for practical SERS applications.

## 5 Supplementary

In order to illustrate the pillar height effect on the electric field intensity distribution, different heights of SiNWs from 50 nm to 800 nm at a step of 50 nm are simulated at the excitation wavelength of 532 nm. As shown in Fig. S1(a), in the FDTD simulations, to calculate electric field enhancement ( $E/E_0$ ), point monitor 1 is placed at the edge top layer of Au disk and point monitor 2 is put at the middle fringe of SiO<sub>2</sub> layer. Fig. S1(b) demonstrates these two groups of the calculated electric field enhancement factors at 532 nm as a function of pillar height. As can be seen, the peak or dip value of electric field enhancement shows a periodic variation of around 250 nm pillar height. The reason for this phenomenon is that the SiNWs introduce constructive or destructive interference between the incident and reflected light. Since the scattering of reflected light may probably increase the light propagation path, the period of SiNWs is slightly smaller than  $\lambda/2$ , where  $\lambda$  is the excitation wavelength.

Although several literatures have reported the pillar height dependent electric field enhancement, their pillar height variation ranges are small (less than 250 nm). Therefore, only the first-order constructive interference is observed [7-8, 25]. Manohar et al demonstrated free-standing nanostar dimers on SiNWs, where electric field enhancement between the nanogaps of dimers reaches the maximum when pillar height is around 150 nm [8]. Since

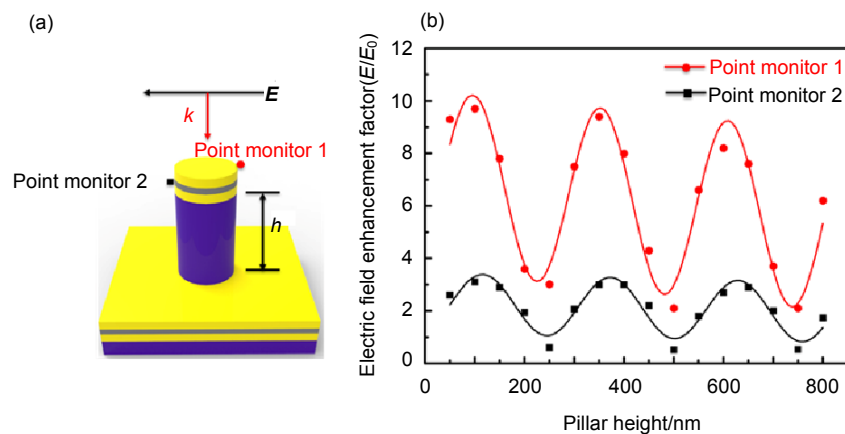


Fig.S1 (a) Sketch of a single hybrid structure, where thicknesses of Au-SiO<sub>2</sub>-Au layers are 25-20-25 nm with period of 500 nm, diameter of 200 nm and height of  $h$ . Point monitors 1 and 2 denote the simulated regions. (b) Calculated electric field enhancement ( $E/E_0$ ) at the excitation wavelength of 532 nm as a function of pillar height from 50 to 800 nm at a step of 50 nm.

the high aspect ratio of SiNWs is able to provide larger surface areas, which allow the decoration of more metal nanoparticles on the sidewalls and thus result in a higher density of hot spots, the increase in hot spots density contributes to stronger SERS signals. Therefore, if both pillar height dependent electric field enhancement and high aspect ratio of pillars with large surface area are considered, larger SERS enhancement factors are expected to be achieved.

## Acknowledgements

The authors would like to acknowledge the financial support from A\*STAR, SERC 2014 Public Sector Research Funding (PSF) Grant (SERC Project No. 1421200080).

## References

- Kneipp K, Wang Yang, Kneipp H, *et al.* Single molecule detection using surface-enhanced Raman scattering (SERS)[J]. *Physical Review Letters*, 1997, **78**(9): 1667–1670.
- Campion A, Kambhampati P. Surface-enhanced Raman scattering[J]. *Chemical Society Reviews*, 1998, **27**(4): 241–250.
- Quyen T T B, Chang C C, Su W N, *et al.* Self-focusing Au@SiO<sub>2</sub> nanorods with rhodamine 6G as highly sensitive SERS substrate for carcinoembryonic antigen detection[J]. *Journal of Materials Chemistry B*, 2014, **2**(6): 629–636.
- Wang Yan, Zhang Xiujuan, Gao Peng, *et al.* Air heating approach for multilayer etching and roll-to-roll transfer of silicon nanowire arrays as SERS substrates for high sensitivity molecule detection[J]. *ACS Applied Materials & Interfaces*, 2014, **6**(2): 977–984.
- Xu Kaichen, Zhang Chentao, Zhou Rui, *et al.* Hybrid micro/nano-structure formation by angular laser texturing of Si surface for surface enhanced Raman scattering[J]. *Optics Express*, 2016, **24**(10): 10352–10358.
- Indrasekara A S D S, Meyers S, Shubeita S, *et al.* Gold nanostar substrates for SERS-based chemical sensing in the femtomolar regime[J]. *Nanoscale*, 2014, **6**(15): 8891–8899.
- Dmitriev A, Hägglund C, Chen Si, *et al.* Enhanced nanoplasmonic optical sensors with reduced substrate effect[J]. *Nano Letters*, 2008, **8**(11): 3893–3898.
- Chirumamilla M, Toma A, Gopalakrishnan A, *et al.* 3D nanostar dimers with a sub-10-nm gap for single-/few-molecule surface-enhanced Raman scattering[J]. *Advanced Materials*, 2014, **26**(15): 2353–2358.
- Hatab N A, Hsueh C H, Gaddis A L, *et al.* Free-standing optical gold bowtie nanoantenna with variable gap size for enhanced Raman spectroscopy[J]. *Nano Letters*, 2010, **10**(12): 4952–4955.
- Ding Li, Qin Jin, Guo Songpo, *et al.* Resonant effects in nano scale bowtie apertures[J]. *Scientific Reports*, 2016, **6**: 27254.
- Yan Zhendong, Du Wei, Tu Linlin, *et al.* A facile high-performance SERS substrate based on broadband near-perfect optical absorption[J]. *Journal of Raman Spectroscopy*, 2015, **46**(9): 795–801.
- Cinel N A, Bütün S, Ertaş G, *et al.* 'Fairy chimney'-shaped tandem metamaterials as double resonance SERS substrates[J]. *Small*, 2013, **9**(4): 531–537.
- Chu Yizhuo, Banaee M G, Crozier K B. Double-resonance plasmon substrates for surface-enhanced Raman scattering with enhancement at excitation and stokes frequencies[J]. *ACS Nano*, 2010, **4**(5): 2804–2810.
- Wells S M, Merkulov I A, Kravchenko I I, *et al.* Silicon nanopillars for field-enhanced surface spectroscopy[J]. *ACS Nano*, 2012, **6**(4): 2948–2959.
- Li Wendi, Ding Fei, Hu J, *et al.* Three-dimensional cavity nanoantenna coupled plasmonic nanodots for ultrahigh and uniform surface-enhanced Raman scattering over large area[J]. *Optics Express*, 2011, **19**(5): 3925–3936.
- Polemi A, Wells S M, Lavrik N V, *et al.* Local field enhancement of pillar nanosurfaces for SERS[J]. *The Journal of Physical Chemistry C*, 2010, **114**(42): 18096–18102.
- Yang J, Li J B, Gong Q H, *et al.* High aspect ratio SiNW arrays with Ag nanoparticles decoration for strong SERS detection[J]. *Nanotechnology*, 2014, **25**(46): 465707.
- Yang Jing, Luo Fangfang, Kao T S, *et al.* Design and fabrication of broadband ultralow reflectivity black Si surfaces by laser micro/nanoprocessing[J]. *Light: Science & Applications*, 2014, **3**(7): e185.
- Seo K, Borguet E. Potential-induced structural change in a self-assembled monolayer of 4-methylbenzenethiol on Au(111)[J]. *The Journal of Physical Chemistry C*, 2007, **111**(17): 6335–6342.
- Li Weiyang, Camargo P H C, Au L, *et al.* Etching and dimerization: a simple and versatile route to dimers of silver nanospheres with a range of sizes[J]. *Angewandte Chemie International Edition*, 2010, **49**(1): 164–168.
- Cai W B, Ren B, Li X Q, *et al.* Investigation of surface-enhanced Raman scattering from platinum electrodes using a confocal Raman microscope: dependence of surface roughening pretreatment[J]. *Surface Science*, 1998, **406**(1-3): 9–22.
- Toussaint K C, Jr, Roxworthy B J, Michaud S, *et al.* Plasmonic nanoantennas: from nanotweezers to plasmonic photography[J]. *Optics and Photonics News*, 2014, **26**(6): 24–31.
- Lévêque G, Martin O J F. Tunable composite nanoparticle for plasmonics[J]. *Optics Letters*, 2006, **31**(18): 2750–2752.
- Liu C H, Hong M H, Cheung H W, *et al.* Bimetallic structure fabricated by laser interference lithography for tuning surface plasmon resonance[J]. *Optics Express*, 2008, **16**(14): 10701–10709.
- Zhang Weihua, Ding Fei, Chou S Y. Large enhancement of upconversion luminescence of NaYF<sub>4</sub>: Yb<sup>3+</sup>/Er<sup>3+</sup> nanocrystal by 3D plasmonic nano-antennas[J]. *Advanced Materials*, 2012, **24**(35): OP236–OP241.